Synthesis, Characterization, and Structure of Neutral and Anionic Complexes Containing Octahedral W_6Te_8 Cluster Units

Xiaobing Xie and Robert E. McCarley*

Ames Laboratory, USDOE, and Department of Chemistry, Iowa State University, Ames, Iowa 50011

Received January 10, 1997[⊗]

The first examples of molecular telluride complexes, $W_6Te_8L_6$ [L =pyridine (py), piperidine (pip), and PEt_3], and the reduced salt $[Na(py)_6]^+[W_6Te_8(py)_6]^-$ were discovered. The amine complexes were prepared by reaction of W_6Cl_{12} with Na_2Te or a Na_2Te/Na_2Te_2 mixture in the amine solvents, whereas $W_6Te_8(PEt_3)_6$ was established by displacement of pyridine in $W_6Te_8(py)_6$ by PEt_3. The cluster unit, W_6Te_8, showed characteristic T_{1u} W−Te stretching vibrations around 180−200 cm^{-1}. From XPS the $W4f_{7/2}$ binding energy of 30.8 eV for $W_6Te_8L_6$ compared favorably with values of 30.5 and 30.8 eV for the sulfide and selenide analogues, respectively. Crystallographic data for the three compounds on which structure analyses were performed are as follows: $W_6Te_8(pip)_6$·6pip, hexagonal, $R\bar{3}$, $a = 17.738(6)$ Å, $c = 24.318(10)$ Å, $Z = 3$; $W_6Te_8(PEt_3)_6$, monoclinic, $C2/c$, $a = 24.724(6)$ Å, $b = 19.716(4)$ Å, $c = 13.543(9)$ Å, $\beta = 108.56(3)°$, $Z = 4$; $[Na(py)_6]^+[W_6Te_8(py)_6]^-$·py, triclinic, $P\bar{1}$, $a = 12.433(3)$ Å, $b = 12.760(2)$ Å, $c = 12.882(2)$ Å, $\alpha = 96.78(1)°$, $\beta = 100.03(1)°$, $\gamma = 98.58(1)°$, $Z = 1$. The average W−Te bond distance of 2.753 Å is very close to the average W−W bond distance of 2.748 Å in these telluride clusters. For the anionic complex, both the small distortion of the octahedral cluster unit and the shortening of the average W−W bond distance confirmed addition of the extra electron to a bonding orbital in the reduced 21e cluster unit. Extended Hückel MO calculations indicate that the structural distortion of the $[W_6Te_8(py)_6]^-$ anion arises from the Jahn−Teller effect on the ^2E_g ground state. The unique cationic unit $[Na(py)_6]^+$ is the first documented example of a sodium ion octahedrally coordinated with six pyridine molecules.

Introduction

The chemistry of molecular tungsten chalcogenide complexes with W_6Q_8 (Q = chalcogen atom) cluster units has attracted considerable interest. These compounds are closely related to the well-known molybdenum chalcogenide Chevrel phases, M_x-Mo_6Q_8, which exhibit diverse and interesting physical and chemical properties.[1−4] The preparation of the Chevrel phases has generally involved solid-state reactions at higher temperatures (1000−1300 °C). However, there presently is no reported example of the tungsten analogues of the Chevrel phases, W_6Q_8 or $M_xW_6Q_8$. It is generally understood that these compounds are unstable at high temperatures with respect to disproportionation (into W and WQ_2 or W, WQ_2, and $MQ_{n/2}$, where n is the valence of M). Thus, these phases may be isolated only at lower temperatures where they are either thermodynamically stable or metastable and kinetically trapped.

Recently, lower temperature synthetic routes via solution precursors have received a good deal of attention. Such routes not only provide a way to produce thin films, coatings, and small particles, either by themselves or on typical catalyst support materials, but also provide opportunities to approach metastable materials. Therefore, W_6Q_8 or $M_xW_6Q_8$ might be obtained through these lower temperature synthetic routes.

The coordination chemistry of molecular molybdenum sulfide[5−7] and selenide[8] cluster complexes has been well-developed. Also, recently, the preparation of molecular tungsten analogues for both the sulfide[9−11] and selenide[12] complexes were reported by our group. However, no example of the corresponding telluride molecular cluster complexes, such as $M_6Te_8L_6$ (M = Mo, W), has been reported. Furthermore, we have become especially interested in the possible low-temperature conversion of these $W_6Q_8L_6$ complexes into the W_6Q_8 or $M_xW_6Q_8$ analogues of the Chevrel phase structure. However, this conversion has not yet been possible with the W_6S_8 and W_6Se_8 cluster complexes.[10c] We wished to examine the W_6Te_8 complexes for this purpose with the idea that the W_6Te_8 binary compound might be more stable toward disproportionation than the W_6S_8 and W_6Se_8 examples. The present paper describes the syntheses, characterizations, and structures of the new neutral molecular complexes of the tungsten telluride clusters $W_6Te_8(pip)_6$ (pip = piperidine),[13] $W_6Te_8(py)_6$ (py = pyridine), and $W_6Te_8(PEt_3)_6$, as well as a reduced ionic compound, $[Na(py)_6]^+[W_6Te_8(py)_6]^-$.[13]

Experimental Section

Materials. Because all reagents and products are air and moisture sensitive, all manipulations were performed by the use of an inert-

[⊗] Abstract published in *Advance ACS Abstracts,* September 15, 1997.

(1) Chevrel, R.; Sergent, M. In *Topics in Current Physics*; Fischer, Ø., Maple, M. B., Eds.; Springer-Verlag: Heidelberg, Germany, 1982; Vol. 32, Chapter 2.
(2) Peña, O.; Sergent, M. *Prog. Solid State Chem.* **1989**, *19*, 165.
(3) Mulhern, P. J.; Haering, R. R. *Can. J. Phys.* **1984**, *62*, 527.
(4) (a) McCarty, K. F.; Schrader, G. L. *Ind. Eng. Chem. Prod. Res. Dev.* **1984**, *23*, 519. (b) McCarty, K. F.; Anderegg, J. W.; Schrader, G. L. *J. Catal.* **1985**, *93*, 375.
(5) Hilsenbeck, S. J.; Young, V. G., Jr.; McCarley, R. E. *Inorg. Chem.* **1994**, *33*, 1822.
(6) (a) McCarley, R. E.; Laughlin, S. K.; Spink, D. A.; Hur, N. *Abstracts of Papers*, 3rd Chemical Congress of North America, Toronto, Ontario, Canada, 1988; American Chemical Society: Washington, DC, 1988. (b) Zhang, X.; Hur, N.; Spink, D. A.; Michel, J. B.; Laughlin, S. K.; McCarley, R. E. Manuscript in preparation.
(7) Saito, T.; Yamamoto, N.; Yamagata, T.; Imoto, H. *J. Am. Chem. Soc.* **1988**, *110*, 1646.
(8) Saito, T.; Yamamoto, N.; Nagase, T.; Tsuboi, T.; Kobayashi, K.; Yamagata, T.; Imoto, H.; Unoura, K. *Inorg. Chem.* **1990**, *29*, 746.
(9) Saito, T.; Yoshikawa, A.; Yamagata, T.; Imoto, H.; Unoura, K. *Inorg. Chem.* **1989**, *28*, 3588.
(10) (a) Zhang, X.; McCarley, R. E. *Inorg. Chem.* **1995**, *34*, 2678. (b) Zhang, X. Ph.D. Dissertation, Iowa State University, Ames, IA, 1991. (c) Xie, X.; McCarley, R. E. Unpublished research.
(11) Ehrlich, G. M.; Warren, C. J.; Vennos, D. A.; Ho, D. H.; Haushalter, R. C.; DiSalvo, F. J. *Inorg. Chem.* **1995**, *34*, 4454.
(12) Xie, X.; McCarley, R. E. *Inorg. Chem.* **1995**, *34*, 6124.
(13) Xie, X.; McCarley, R. E. *Inorg. Chem.* **1996**, *35*, 2713.

S0020-1669(97)00037-2 CCC: $14.00

atmosphere drybox, a high-vacuum manifold, and Schlenk techniques, unless otherwise stated. W_6Cl_{12} was prepared by literature methods.[10b,14] Na_2Te and Na_2Te_2 were prepared by the reactions of the stoichiometric amount of elemental sodium and tellurium in liquid NH_3.[15] All solvents were purified and dried prior to use. Also, the solvents were deoxygenated by use of the freeze−thaw process: freeze to liquid nitrogen temperature, evacuate the gaseous material, and then thaw. This process was repeated three times prior to the distillation of the purified solvent onto Linde 3- or 4-Å molecular sieves and stored under vacuum or a nitrogen atmosphere. Pyridine (Fisher), piperidine (Fisher), and triethylphosphine (Strem) were purified by refluxing over calcium hydride for at least 4 h. Toluene (Fisher) and chloroform were refluxed over phosphorus pentoxide. Without heating, tetrahydrofuran (Fisher) was stirred with sodium metal and a benzophenone indicator. Methanol (Mallinckrodt) was dried by refluxing over sodium methoxide. When used, the solvents were vacuum-distilled or syringed under a flowing nitrogen gas atmosphere.

Physical Measurements. Infrared (4000−200 cm^{-1}) spectra were recorded with a Bomem MB-102 Fourier transform infrared spectrometer manufactured by Hartman and Braun. Mineral oil mulls of samples were pressed between two cesium iodide plates. Far-infrared (650−100 cm^{-1}) spectra were recorded separately with an IBM IR/98 Fourier transform infrared spectrometer. Thick sample mulls were placed on a polyethylene film. XP spectra were collected with a Physical Electronics Industries 5500 multitechnique surface analysis system, and binding energies were calibrated with C 1s = 284.6 eV. Powder X-ray diffraction (XRD) data were obtained with a Philips ADP3520 $\theta-2\theta$ diffractometer using Cu Kα radiation. The air-sensitive samples were loaded into a specially designed sample holder that was sealed under inert atmosphere. Electronic spectra were collected on a Hewlett-Packard 8453 UV−vis scanning spectrophotometer. The samples of $W_6Q_8(pip)_6$ (Q = S, Se, Te) were dissolved in neat piperidine and examined over the range 300−1000 nm. A piperidine blank was used as the reference and subtracted from the sample spectra. The magnetic properties were examined on powder samples with a Quantum SQUID magnetosusceptometer. ESR spectra were recorded using a Bruker ESP-300 spectrometer. ^{31}P and ^{1}H NMR spectra were obtained on a Bruker AC 200 spectrometer.

Analytical Procedures. Tungsten was determined gravimetrically as the trioxide. The samples were dissolved in 0.5 M KOH basic solutions with the aid of hydrogen peroxide. The solutions were then treated with concentrated nitric acid and 2 mL of hydrogen peroxide to form a peroxy acid complex. The hydrated oxide, $WO_3 \cdot nH_2O$, was then completely precipitated by slowly decomposing the solution of this complex at 100 °C and collected in a tared ceramic filter crucible. After washing with dilute nitric acid and hydrochloric acid extensively to remove any TeO_2 or TeO_3 residues, the materials were heated to constant weight at 800 °C. Chlorine was determined by potentiometric titration with a standardized silver nitrate solution after dissolving the samples in hot KOH/H_2O_2 solutions and neutralization.

Synthetic Procedures. Preparation of $W_6Te_8(pip)_6 \cdot 6pip$. W_6Cl_{12} (0.300 g, 0.196 mmol), Na_2Te (0.136 g, 0.784 mmol), and Na_2Te_2 (0.118 g, 0.392 mmol) were weighed in the drybox and transferred into a 100-mL Schlenk reaction flask equipped with a water-cooled condenser. By distillation, 40 mL of piperidine was added to the reactants, and the mixture was refluxed for 3 days. A black solid and dark-blue solution were separated by filtration. Single crystals of $W_6Te_8(pip)_6 \cdot 6pip$ were grown from a portion of the filtrate by allowing it to stand at −20 °C for several weeks. The solvent was removed from the remainder of the filtrate under dynamic vacuum, and about 0.35 g of dark blue powder was recovered. This procedure resulted in partial removal of the lattice-bound piperidine. Anal. Calcd for $W_6Te_8(pip)_6 \cdot 2pip$: W, 39.32. Found: W, 39.78. A test for chloride was negative. UV−vis (λ, piperidine): 566 nm.

Preparation of $W_6Te_8(py)_6$. W_6Cl_{12} (0.300 g, 0.196 mmol), Na_2Te (0.136 g, 0.784 mmol), and Na_2Te_2 (0.118 g, 0.392 mmol) were weighed in the drybox and transferred into a 100-mL Schlenk reaction flask equipped with a water-cooled condenser. By distillation, 50 mL of pyridine was added to the reactants, and the mixture was refluxed for 3 days. The black insoluble product solid was isolated by filtration and then extracted with methanol for 2 days to remove the NaCl byproduct. About 0.45 g of black powder (88% yield) was thereby recovered after being dried under dynamic vacuum for 1 day. All attempts to grow single crystals of this insoluble compound were unsuccessful. IR (Nujol, cm^{-1}): 1594 (w), 1348 (w), 1306 (w), 1208 (s), 1168 (w), 1146 (m), 1063 (ms), 1035 (ms), 965 (w), 932 (w), 746 (s), 685 (s), W−Te 180 (ms). A test for chloride was negative. Anal. Calcd for $W_6Te_8(py)_6$: W, 42.45. Found: W, 40.6.

Preparation of $W_6Te_8(PEt_3)_6$. About 0.24 g of $W_6Te_8(pip)_6$ was loaded into a 100 mL Schlenk reaction flask equipped with a water-cooled condenser. By syringe, 40 mL of toluene and 0.15 mL of triethylphosphine were added, and the mixture was refluxed for 1 day. The mixture was filtered while hot, thereby providing a small amount of solid and a grape purple solution. The toluene was then removed from the filtrate under dynamic vacuum, and after overnight drying *in vacuo*, 0.22 g of dark purple powder was collected. IR (Nujol, cm^{-1}): 1255 (m), 1168 (w), 1146 (m), 1033 (s), 759 (s), 713 (m), 404 (ms), 368 (s), 334 (w), W−Te 205 (m). $^{31}P\{^{1}H\}$ NMR (C_6D_6): $\delta = -44.0$ (s). ^{1}H NMR (C_6D_6): $\delta = 0.64-0.81$ (m, CH_3), 1.23−1.40 (m, CH_2). Chemical shifts are relative to 85% H_3PO_4 and TMS, respectively. Single crystals of $W_6Te_8(PEt_3)_6$ for X-ray diffraction were obtained by redissolving 0.05 g of the purple solid in 6 mL of $CHCl_3$ and allowing the solution to stand at −20 °C for 1 week. There was insufficient material for chemical analysis.

Preparation of $[Na(py)_6][W_6Te_8(py)_6] \cdot py$. W_6Cl_{12} (0.500 g, 0.327 mmol) and Na_2Te (0.453 g, 2.610 mmol) were weighed in the drybox and transferred into a 100-mL Schlenk reaction flask equipped with a water-cooled condenser. By vacuum distillation, 50 mL of pyridine was added to the reactants, and the mixture was refluxed for 2 days. The mixture was then filtered while hot, and 0.622 g of a black solid and dark red solution were separated. Single crystals of $[Na(py)_6][W_6Te_8(py)_6] \cdot py$ were grown from the filtrate solution by allowing it to stand at room temperature for 2 days. Analytical data for these crystals could not be obtained because of their facile loss of pyridine upon handling. After separation of the crystals, a further 0.41 g of black powder was recovered upon removal of solvent from the solution. A test for chloride on this material was negative. The black insoluble product obtained by filtration of the reaction mixture was washed with methanol for 2 days to remove the NaCl byproduct, and about 0.25 g of black solid was recovered. A test for chloride was negative.

Reaction of $W_6Te_8(pip)_6$ with Pyridine. About 0.20 g of the piperidine adduct $W_6Te_8(pip)_6$ was weighed in the drybox and transferred into a 100 mL Schlenk reaction flask, and 30 mL of pyridine was vacuum-distilled onto the solid. The solid was initially soluble in pyridine. After the mixture was refluxed for several hours or allowed to sit at room temperature for 2 days, a black solid and faintly colored filtrate were obtained upon filtration. The black powder was then recovered and dried *in vacuo*. The IR spectrum of this black powder was identical to that of $W_6Te_8(py)_6$. IR (Nujol, cm^{-1}): 1594 (w), 1348 (w), 1306 (w), 1208 (s), 1168 (w), 1146 (m), 1063 (ms), 1035 (ms), 965 (w), 932 (w), 746 (s), 685 (s), W−Te 182 (ms).

X-ray Structure Determinations. Single-crystal structure determinations were undertaken for three of the $W_6Te_8L_6$ cluster complexes. In each case, a crystal was chosen from material still in contact with the mother solution. The crystals were encased in epoxy cement, quickly attached to the tip of a glass fiber, and immediately inserted into the low-temperature nitrogen stream of the diffractometer for data collection. The cell constants were determined from 25 randomly located and centered reflections. The structures were solved by direct methods using SHELXS[16] and refined on *F* by full-matrix, least-squares techniques with the TEXSAN package.[17] Pertinent crystallographic data are listed in Table 1.

(14) Ehrlich, G. M.; Rauch, P. E.; DiSalvo, F. J. *Inorg. Synth.* **1995**, *30*, 1.
(15) (a) Klemm, W.; Sodomann, H.; Langmesser, P. *Z. Anorg. Allg. Chem.* **1939**, *241*, 281. (b) Fener, F. In *Handbuch der Praparativen Anorganischen Chemie;* Brauer, G., Ed.; Ferdinand Enke: Stuttgart, Germany, 1954; pp 280−281.
(16) Scheldrick, G. M. *Crystallographic Computing 3*; Oxford University Press: Oxford, U.K., 1985.
(17) *TEXSAN: Single Crystal Structure Analysis Software*, Version 1.6c; Molecular Structure Corp.: The Woodlands, TX 77381, 1985 and 1992.

Table 1. Crystallographic Data for the $W_6Te_8L_6$ Cluster Complexes

	$W_6Te_8(pip)_6 \cdot 6pip$	$W_6Te_8(PEt_3)_6$	$[Na(py)_6][W_6Te_8(py)_6] \cdot py$
empirical formula	$C_{70}H_{154}N_{14}Te_8W_6$	$C_{36}H_{90}P_6Te_8W_6$	$C_{65}H_{65}NaN_{13}Te_8W_6$
fw	2926.86	2832.85	3175.21
space group	$R\bar{3}$ (No.148)	$C2/c$ (No.15)	$P\bar{1}$ (No. 2)
a, Å	17.738(6)	24.724(6)	12.433(3)
b, Å		19.716(4)	12.760(2)
c, Å	24.318(10)	13.543(9)	12.882(2)
α, deg			96.78(1)
β, deg		108.56(3)	100.03(1)
γ, deg			98.58(1)
V, Å^3	6638(2)	6258(4)	1968(1)
Z	3	4	1
ρ_{calcd}, g/cm^3	2.361	3.006	2.679
μ, cm^{-1}	103.99	148.30	116.99
λ(Mo Kα), Å	0.710 69	0.710 69	0.710 69
T, °C	−70	−70	−70
R^a	0.045	0.027	0.034
$R_w{}^b$	0.041	0.030	0.030

[a] $R = \sum||F_o| - |F_c||/\sum|F_o|$. [b] $R_w = [\sum w(|F_o| - |F_c|)^2/\sum w|F_o|^2]^{1/2}$; $w = 1/\sigma^2(|F_o|)$.

Structure Determination for $W_6Te_8(pip)_6 \cdot 6pip$. A black crystal, with dimensions of 0.20 × 0.30 × 0.35 mm^3, was mounted on a glass fiber. Data were collected with a Rigaku AFC6R diffractometer using Mo Kα radiation, over the range $4° < 2\theta < 45°$ in the hemisphere ($\pm h,+k,\pm l$) using the $\omega-2\theta$ scan technique. Three standard reflections were monitored every 150 reflections and showed no intensity variation over the collection period. A total of 3294 reflections were collected, of which 1938 were unique ($R_{int} = 0.068$) and 1203 were observed with $I > 3\sigma(I)$. First, an empirical absorption correction using the φ scan technique was applied after the structure solution. After all of the atoms were located and refined isotropically, the φ scan absorption correction was removed, and an absorption correction using the DIFABS program[18] was applied, resulting in relative transmission factors ranging from 0.88 to 1.11. The data were corrected for Lorentz and polarization effects.

The trigonal space group $R\bar{3}$ was chosen on the basis of systematic absences and intensity statistics. Initial tungsten atom positions were input on the basis of the SHELXS direct methods[16] output. Subsequently, the other non-hydrogen atomic positions were located directly from the electron density difference maps. These atoms were refined with anisotropic thermal parameters, except the nitrogen atom on the piperidine ligand molecule. Idealized hydrogen positions were calculated and placed in the refinement with C−H distances equal to 1.04 Å and N−H distances equal to 0.96 Å, but their parameters were held constant during subsequent cycles. The final cycle of full-matrix least-squares refinement was based on 1203 observed reflections and 125 variable parameters and converged with unweighted and weighted agreement factors of $R = 0.045$ and $R_w = 0.041$, respectively. The asymmetric unit was found to be $WTe_2(pip) \cdot pip$. One of the tellurium atoms is located at a special position (3c), and all the other unique atoms are at general positions. The atomic coordinates and equivalent isotropic thermal parameters of the non-hydrogen atoms are given in Table 2.

Structure Determination for $W_6Te_8(PEt_3)_6$. Single crystals were grown from a chloroform solution of $W_6Te_8(PEt_3)_6$ upon standing at −20 °C. A black crystal, with dimensions of 0.10 × 0.20 × 0.35 mm^3, was mounted on a glass fiber. Data were collected with a Rigaku AFC6R diffractometer using Mo Kα radiation, over the range $4° < 2\theta < 55°$ in the hemisphere ($\pm h,\pm k,+l$) using the $\omega-2\theta$ scan technique. Three standard reflections were monitored every 200 reflections and showed 1.99% intensity decay over the collection period. A total of 15 087 reflections were collected, of which 7465 were unique ($R_{int} = 0.083$) and 3361 were observed with $I > 5\sigma(I)$. First, an empirical absorption correction using the φ scan technique was applied after the structure solution. After all of the atoms were located and refined isotropically, the φ scan absorption correction was removed, and an absorption correction using the DIFABS program[18] was applied, resulting in relative transmission factors ranging from 0.81 to 1.22. The data were corrected for Lorentz and polarization effects. A correction for decay (1.99%) and a correction for secondary extinction[19] (coefficient = 1.59×10^{-10}) were also applied.

The monoclinic space group $C2/c$ was chosen on the basis of systematic absences and intensity statistics. Initial tungsten atom positions were input on the basis of the SHELXS direct methods[16] output. Subsequently, the other non-hydrogen atomic positions were located directly from the electron density difference maps. These atoms were refined with anisotropic thermal parameters, except one carbon atom on a ligand molecule. Idealized hydrogen positions were calculated and placed in the refinement with C−H distances equal to 1.06 Å, but their parameters were held constant during subsequent cycles. The final cycle of full-matrix least-squares refinement was based on 3361 observed reflections and 249 variable parameters and converged with unweighted and weighted agreement factors of $R = 0.027$ and $R_w = 0.030$, respectively. The asymmetric unit was found to be $W_3Te_4(PEt_3)_3$. The atomic coordinates and equivalent isotropic thermal parameters of the non-hydrogen atoms are given in Table 3.

Table 2. Atomic Coordinates and Equivalent Isotropic Thermal Parameters (Å^2) for the Non-Hydrogen Atoms of $W_6Te_8(pip)_6 \cdot 6pip$

atom	x	y	z	$B_{eq}{}^a$
W(1)	0.02317(5)	0.09862(5)	0.04597(3)	1.86(2)
Te(1)	0.0000	0.0000	0.13788(8)	2.52(3)
Te(2)	0.04632(9)	0.19766(8)	−0.04723(5)	2.26(3)
N(1)	0.050(1)	0.2211(10)	0.0968(5)	2.3(3)
N(2)	0.282(1)	0.359(1)	−0.0486(8)	4.2(5)
C(11)	0.017(2)	0.204(1)	0.1561(9)	4.2(6)
C(12)	0.022(2)	0.281(2)	0.1854(10)	4.8(7)
C(13)	0.130(2)	0.298(1)	0.0929(9)	4.5(6)
C(14)	0.139(2)	0.379(2)	0.120(1)	5.7(7)
C(15)	0.108(3)	0.360(2)	0.179(1)	7(1)
C(21)	0.266(2)	0.419(2)	−0.086(1)	6.0(8)
C(22)	0.370(3)	0.479(2)	0.013(1)	8.2(10)
C(23)	0.355(3)	0.544(2)	−0.026(1)	9(1)
C(24)	0.270(2)	0.495(2)	−0.058(1)	7(1)
C(25)	0.364(2)	0.406(2)	−0.016(1)	7.3(10)

[a] $B_{eq} = {}^8/_3\pi^2[U_{11}(aa^*)^2 + U_{22}(bb^*)^2 + U_{33}(cc^*)^2 + 2U_{12}aa^*bb^* \cos\gamma + 2U_{13}aa^*cc^* \cos\beta + 2U_{23}bb^*cc^* \cos\alpha]$.

Structure Determination for $[Na(py)_6][W_6Te_8(py)_6] \cdot py$. Single crystals were grown from the pyridine reaction filtrate by allowing it to stand at room temperature. A dark rectangular crystal, with dimensions of 0.20 × 0.20 × 0.40 mm^3, was mounted on a glass fiber. Data were collected with a Rigaku AFC6R diffractometer using Mo Kα radiation, over the range $3° < 2\theta < 55°$ in the hemisphere ($+h,\pm k,\pm l$), using the $\omega-2\theta$ scan technique. Three standard reflections were monitored every 200 reflections and showed no intensity variation over the collection period. A total of 9508 reflections were collected, of which 9101 were unique ($R_{int} = 0.055$) and 4575 were observed

(18) *DIFABS*: Walker, N.; Stuart, D. *Acta Crystallogr.* **1983**, *A39*, 158.

(19) (a) Zachariasen, W. H. *Acta Crystallogr.* **1967**, *23*, 558. (b) Lawrence, J. L. *Acta Crystallogr.* **1977**, *A33*, 232.

Table 3. Atomic Coordinates and Equivalent Isotropic Thermal Parameters (Å^2) for the Non-Hydrogen Atoms of $W_6Te_8(PEt_3)_6$

atom	*x*	*y*	*z*	B_{eq}[a]
W(1)	0.30317(3)	0.18979(3)	0.96151(4)	1.08(1)
W(2)	0.29474(3)	0.32851(3)	0.98399(5)	1.12(1)
W(3)	0.29667(3)	0.24289(3)	1.14673(5)	1.07(1)
Te(1)	0.30360(5)	0.10510(5)	1.12276(7)	1.48(2)
Te(2)	0.39300(4)	0.26074(5)	1.09094(8)	1.40(2)
Te(3)	0.29989(5)	0.27541(5)	0.79932(7)	1.47(2)
Te(4)	0.21254(4)	0.11932(5)	0.83234(7)	1.41(2)
P(1)	0.3758(2)	0.1153(2)	0.9162(3)	1.81(8)
P(2)	0.3544(2)	0.4303(2)	0.9702(3)	2.01(9)
P(3)	0.3559(2)	0.2356(2)	1.3374(3)	1.66(8)
C(111)	0.4144(9)	0.0497(7)	1.013(1)	2.9(4)
C(112)	0.4573(9)	0.0789(8)	1.112(1)	3.7(5)
C(121)	0.3505(8)	0.0612(7)	0.800(1)	2.7(4)
C(122)	0.3286(9)	0.0996(7)	0.695(1)	2.8(4)
C(131)	0.4368(8)	0.1629(8)	0.894(1)	2.7(4)
C(132)	0.4813(10)	0.1216(10)	0.868(2)	4.1(4)
C(211)	0.3859(9)	0.4300(9)	0.868(1)	3.4(5)
C(212)	0.4353(9)	0.375(1)	0.884(2)	4.1(5)
C(221)	0.4138(7)	0.4497(7)	1.094(1)	2.3(4)
C(222)	0.4495(8)	0.5119(7)	1.091(2)	3.0(4)
C(231)	0.3196(8)	0.5129(7)	0.939(1)	3.0(4)
C(232)	0.2945(7)	0.5439(7)	1.022(1)	2.6(4)
C(311)	0.4294(8)	0.2631(9)	1.372(1)	3.0(4)
C(312)	0.4382(8)	0.3403(9)	1.358(1)	3.3(4)
C(321)	0.3309(8)	0.2842(8)	1.429(1)	2.3(4)
C(322)	0.3669(9)	0.2841(9)	1.545(1)	3.5(4)
C(331)	0.3701(8)	0.1502(8)	1.400(1)	2.5(4)
C(332)	0.3149(9)	0.1167(9)	1.406(1)	3.3(4)

[a] $B_{eq} = {}^8/_3\pi^2[U_{11}(aa^*)^2 + U_{22}(bb^*)^2 + U_{33}(cc^*)^2 + 2U_{12}aa^*bb^* \cos\gamma + 2U_{13}aa^*cc^* \cos\beta + 2U_{23}bb^*cc^* \cos\alpha]$.

with $I > 4\sigma(I)$. First, an empirical absorption correction using the φ scan technique was applied after the structure solution. After all of the atoms were located and refined isotropically, the φ scan absorption correction was removed, and an absorption correction using the DIFABS program[18] was applied, resulting in relative transmission factors ranging from 0.73 to 1.47. The data were corrected for Lorentz and polarization effects. And a correction for secondary extinction[19] was applied (coefficient $= 1.17 \times 10^{-8}$).

The triclinic space group $P\bar{1}$ was chosen on the basis of intensity statistics. Initial tungsten atom positions were input on the basis of the SHELXS direct methods[16] output. Subsequently, the non-hydrogen atomic positions were located directly from the electron density difference maps. All non-hydrogen atoms were refined with anisotropic thermal parameters. Idealized hydrogen positions were calculated and placed in the refinement, but their parameters were held constant during subsequent cycles. The final cycle of full-matrix least-squares refinement was based on 4575 observed reflections and 407 variable parameters and converged with unweighted and weighted agreement factors of $R = 0.034$ and $R_w = 0.030$, respectively. The asymmetric unit was found to be $[Na(py)_3][W_3Te_4(py)_3]\cdot 0.5py$. The atomic coordinates and equivalent isotropic thermal parameters of the non-hydrogen atoms are given in Table 4.

Molecular Orbital Calculations. The molecular orbitals were calculated by the extended Hückel method.[20] The H_{ij} parameters and orbital exponents for sulfur, selenium, and tellurium were taken from the literature,[21] and the parameters for W, N, and H were accepted values.[22] The hypothetical complexes $W_6Q_8(NH_3)_6$ (Q = S, Se, Te) were used as models for the EHMO calculations. Distances found from the X-ray crystal structure determinations of the $W_6Q_8(pip)_6$ complexes were averaged and used to generate the geometries of the core ($W_6Q_8N_6$) of the model complexes with O_h symmetry. The actual bond distances used in the MO calculations are listed in Table 5. The idealized hydrogen positions were calculated on the basis of the tetrahedral symmetry around the nitrogen atoms with N−H bond distances of 0.96 Å. The parameters used for the extended Hückel calculations are listed in Table 6.

Table 4. Atomic Coordinates and Equivalent Isotropic Thermal Parameters (Å^2) for the Non-Hydrogen Atoms of $[Na(py)_6][W_6Te_8(py)_6]\cdot py$

atom	*x*	*y*	*z*	B_{eq}[a]
W(1)	−0.07249(5)	−0.00407(5)	−0.14753(5)	1.27(1)
W(2)	0.13300(5)	0.08081(5)	−0.02662(5)	1.19(1)
W(3)	0.05182(5)	−0.13149(5)	−0.03839(5)	1.17(1)
Te(1)	0.01114(8)	0.20940(8)	−0.13843(8)	1.57(2)
Te(2)	0.26042(8)	−0.04729(8)	0.08069(8)	1.78(2)
Te(3)	0.11437(8)	−0.05629(9)	−0.21554(8)	1.85(2)
Te(4)	0.15327(8)	0.21867(8)	0.16201(8)	1.85(2)
Na(1)	0.5000	0.5000	0.5000	2.7(2)
N(1)	−0.1627(10)	−0.0075(10)	−0.3208(9)	2.2(3)
N(2)	0.2929(9)	0.181(1)	−0.0539(10)	2.2(3)
N(3)	0.1130(9)	−0.2887(9)	−0.0816(9)	1.7(3)
N(10)	0.665(1)	0.620(1)	0.462(1)	4.6(4)
N(20)	0.619(1)	0.415(1)	0.646(1)	4.2(4)
N(30)	0.456(1)	0.642(1)	0.635(1)	3.6(4)
C(11)	−0.267(1)	−0.051(1)	−0.353(1)	3.8(4)
C(12)	−0.327(2)	−0.053(2)	−0.458(1)	6.1(6)
C(13)	−0.276(2)	0.000(2)	−0.527(1)	5.9(6)
C(14)	−0.168(2)	0.044(2)	−0.494(1)	5.5(6)
C(15)	−0.115(1)	0.042(1)	−0.390(1)	3.2(4)
C(21)	0.374(1)	0.140(1)	−0.088(1)	2.7(4)
C(22)	0.471(1)	0.195(2)	−0.104(2)	4.7(6)
C(23)	0.487(1)	0.306(2)	−0.081(2)	4.6(5)
C(24)	0.408(1)	0.355(1)	−0.047(1)	3.4(4)
C(25)	0.313(1)	0.287(1)	−0.034(1)	2.7(4)
C(31)	0.051(1)	−0.386(1)	−0.085(1)	2.5(4)
C(32)	0.081(2)	−0.481(1)	−0.116(2)	4.0(5)
C(33)	0.181(2)	−0.483(1)	−0.137(1)	3.7(5)
C(34)	0.249(2)	−0.387(1)	−0.133(1)	3.6(5)
C(35)	0.210(1)	−0.293(1)	−0.109(1)	2.4(4)
C(101)	0.687(2)	0.470(2)	0.731(2)	5.4(6)
C(102)	0.743(2)	0.422(2)	0.806(2)	7.6(8)
C(103)	0.739(2)	0.317(2)	0.796(2)	5.7(7)
C(104)	0.673(3)	0.254(2)	0.703(2)	7.7(9)
C(105)	0.610(2)	0.310(2)	0.636(1)	5.0(6)
C(201)	0.749(2)	0.672(2)	0.535(2)	4.9(6)
C(202)	0.835(2)	0.742(2)	0.515(2)	6.0(6)
C(203)	0.835(2)	0.761(2)	0.414(2)	6.7(7)
C(204)	0.746(2)	0.709(2)	0.333(2)	5.7(7)
C(205)	0.666(2)	0.643(2)	0.362(2)	5.0(6)
C(301)	0.524(1)	0.708(2)	0.714(2)	4.8(6)
C(302)	0.504(2)	0.796(2)	0.767(2)	5.6(6)
C(303)	0.404(2)	0.824(2)	0.747(2)	5.2(6)
C(304)	0.328(2)	0.756(2)	0.671(2)	6.1(7)
C(305)	0.355(1)	0.667(2)	0.616(1)	3.8(5)
C(400)	−0.038(3)	0.462(4)	0.583(3)	11.7(9)
N(400)[b]	−0.038(3)	0.462(4)	0.583(3)	11.7(9)
C(401)[b]	−0.058(3)	0.377(3)	0.487(4)	13(1)
N(401)[b]	−0.058(3)	0.377(3)	0.487(4)	13(1)
C(402)[b]	0.015(3)	0.563(3)	0.592(3)	11.9(9)
N(402)[b]	0.015(3)	0.563(3)	0.592(3)	11.9(9)

[a] $B_{eq} = {}^8/_3\pi^2[U_{11}(aa^*)^2 + U_{22}(bb^*)^2 + U_{33}(cc^*)^2 + 2U_{12}aa^*bb^* \cos\gamma + 2U_{13}aa^*cc^* \cos\beta + 2U_{23}bb^*cc^* \cos\alpha]$. [b] Disordered positions.

Table 5. Bond Distances (Å) in the Model Complexes for EHMO Calculations

formula	W−W	W−Q	W−N	N−H
$W_6S_8(NH_3)_6$	2.659	2.457	2.312	0.96
$W_6Se_8(NH_3)_6$	2.690	2.571	2.276	0.96
$W_6Te_8(NH_3)_6$	2.742	2.753	2.335	0.96

Results and Discussion

Synthesis of $W_6Te_8(py)_6$. Substitution of sulfide for chloride in $M_6Cl_8^{4+}$ cluster units (M = Mo, W) has been extensively investigated earlier in this research group. Previous research

(20) Hoffman, R. J. *J. Chem. Phys.* **1963**, *39*, 1397.
(21) Beuze, A. L.; Loirat, H.; Zerrouki, M. C.; Lissillour, R. *J. Solid State Chem.* **1995**, *120*, 80.
(22) (a) Atomic orbital ζ parameters were taken from the following: Clementi, E.; Roetti, C. *At. Data Nucl. Data Tables* **1974**, *14*, 177. (b) H_{ii} parameters were taken from the following: Moore, C. Circular 467; U.S. Department of Commerce, National Bureau of Standards: Washington, DC, 1949; Vols. 1−3.

Table 6. Parameters Used in the Extended Hückel Calculations

orbital		H_{ii}, eV	ζ_1	ζ	C_1	C_2
S	3s	−20.00	2.12			
	3p	−13.30	1.83			
Se	4s	−20.50	2.44			
	4p	−13.05	2.07			
Te	5s	−20.5	2.57			
	5p	−12.9	2.16			
W	6s	−8.26	2.34			
	6p	−5.17	2.31			
	5d	−10.37	4.98	2.070	0.6683	0.5422
N	2s	−26.00	1.95			
	2p	−13.40	1.95			
H	1s	−13.60	1.30			

showed that NaSH was a good sulfiding agent, as well as an oxidizing agent.[10] Zhang and McCarley demonstrated that the completely sulfide-substituted hexatungsten cluster $W_6S_8(py)_6$ could be formed by reaction of W_6Cl_{12}, NaSH, and $NaOBu^n$ in a 1:12:6 ratio in refluxing pyridine.[10] During sulfidation, the 24 e clusters ($M_6Cl_8^{4+}$) were oxidized to 20 e clusters (W_6S_8). Pyridine was used as the solvent since it possessed a sufficiently high boiling point to conveniently promote the reaction at reflux temperatures and acted as a good ligand for binding in the terminal positions of the W_6S_8 cluster units, thus stabilizing the cluster complex.

However, for the telluride reactions, NaTeH was not available. Sodium telluride (Na_2Te) and sodium ditelluride (Na_2Te_2) together were chosen as the tellurium source, with the expectation that sodium ditelluride (Na_2Te_2) could also serve as a mild oxidizing agent, like NaSH in the sulfide system. The expected overall reaction is given by eq 1.

$$W_6Cl_{12} + 4Na_2Te + 2Na_2Te_2 + 6py \rightarrow W_6Te_8(py)_6 + 12NaCl \quad (1)$$

The above stoichiometric reaction was conducted in refluxing pyridine. After the reaction, the faint color of the filtrate indicated that the products were all insoluble. Following a prolonged methanol extraction of the products to remove the NaCl byproduct, a black amorphous material was obtained. The presence of only one doublet in the tungsten 4f XPS with appropriate binding energy ($4f_{7/2}$ 30.8 eV) confirmed that the W_6Te_8 cluster was a structural unit in this material. Furthermore, no sodium was detected by XPS. On the basis of tungsten analysis and XPS and IR studies, we determined that the $W_6Te_8(py)_6$ complex was obtained from this reaction, in a yield of about 88%.

All attempts to grow single crystals of this compound were unsuccessful. Compared with its sulfide and selenide analogues, this $W_6Te_8(py)_6$ complex is much more insoluble in most organic solvents and much more air and moisture sensitive. For example, the material burst into flames immediately upon exposure to air.

Synthesis of $W_6Te_8(pip)_6$. The preparation of the piperidine complex, $W_6Te_8(pip)_6$, was similar to that of the pyridine complex, except that the reaction was conducted in neat piperidine instead of pyridine. In contrast to the insolubility of the pyridine complex, the product obtained from this reaction was quite soluble in the amine solvent. After the reaction mixture was refluxed for 2 days and filtered, a dark blue solution was obtained. Single crystals of $W_6Te_8(pip)_6 \cdot 6pip$ were grown from this solution. From the insoluble portion of the reaction mixture was recovered a black solid after removal of NaCl by extraction with MeOH. Examination of this solid by XPS indicated that it contained at least three different kinds of tungsten, and it appeared that the cluster unit, WTe_2, and WO_3 were all present on the basis of their W $4f_{7/2}$ binding energy (eV) values.

Thus, in comparison, this reaction was not as clean and quantitative as the reaction conducted in pyridine. However, solubility of the desired product in piperidine provided an easy separation from the other, insoluble products. This piperidine complex is also very air and moisture sensitive.

Synthesis of $[Na(py)_6]^+[W_6Te_8(py)_6]^-$. Previous research on selenide substitutions in the $(W_6Cl_8)^{4+}$ cluster units (W_6Cl_{12}) showed that Na_2Se was a good selenium source.[12] The neutral molecular complexes $W_6Se_8(py)_6$ and $W_6Se_8(pip)_6$ were obtained when 8 mol of Na_2Se reacted with 1 mol of W_6Cl_{12} in refluxing pyridine and piperidine, respectively.

Thus, if 8 mol of Na_2Te were reacted with 1 mol of W_6Cl_{12}, the neutral telluride cluster complexes $W_6Te_8L_6$ would be expected to form. However, for the reactions conducted in 1:8 mole ratio in pyridine, the material recovered from the filtrate was an ionic compound, $[Na(py)_6]^+[W_6Te_8(py)_6]^-$, on the basis of single-crystal X-ray diffraction, ESR, and XPS. When the insoluble residue of the reaction was washed with MeOH for 2 days to remove NaCl, a quantity of the neutral cluster compound $W_6Te_8(py)_6$ was also recovered, on the basis of XPS and IR spectra. It is evident that both the neutral W_6Te_8 and the ionic cluster core $W_6Te_8^-$ are formed in either piperidine or pyridine. In the case of the 1:8 $W_6Cl_{12}-Na_2Te$ reaction in piperidine, single crystals of $W_6Te_8(pip)_6 \cdot 6pip$ were crystallized from the reaction filtrate; however, sodium was also detected in this filtrate by XPS. Owing to the relatively high solubility of $W_6Te_8(pip)_6$ in piperidine, both the neutral and the ionic complexes were together in solution. However, only the neutral one could be crystallized. In the reaction in pyridine, the ionic compound, $[Na(py)_6]^+ [W_6Te_8(py)_6]^-$, is soluble and remains in the filtrate, while the neutral complex, $W_6Te_8(py)_6$, remains in the insoluble residue.

Mechanism of the Reactions. Ideally, if Na_2Q were used as the chalcogen source instead of NaQH, it would lead to the formation of $W_6Q_8^{4-}$ or $W_6Q_8L_6^{4-}$ as indicated by eq 2, since

$$W_6Cl_{12} + 8Na_2Q \xrightarrow{L} Na_4W_6Q_8L_6 + 12NaCl \quad (2)$$

Na_2Q cannot serve as an oxidizing agent. However, the material isolated from the reactions contained the neutral cluster molecules $W_6Q_8(pip)_6$ or $W_6Q_8(py)_6$ (Q = Se, Te) or the anionic cluster $W_6Te_8L_6^-$, on the basis of spectroscopic analyses (XPS and IR) and X-ray diffraction. What is the oxidizing agent in these reactions?

One possibility is that sodium polychalcogenides (Na_2Q_x, $x \geq 2$) are present as impurities in the reactant Na_2Q and thus oxidize the cluster units. However, the sodium chalcogenides (Na_2Q) were prepared by reacting the chalcogen element with a slight excess of sodium metal to prevent the formation of the polychalcogenides. The XRD patterns of these sodium chalcogenides (Na_2Q, Q = Se, Te) match the known patterns of the corresponding pure compounds. Therefore, this possibility can be ruled out.

Another possibility is that the 24-electron $(W_6Q_8)^{4-}$ unit undergoes disproportionation to form elemental tungsten and the 20-electron neutral cluster $W_6Q_8L_6$, as indicated in eq 3.

$$Na_4W_6Q_8L_6 \rightarrow {}^3/_4W_6Q_8L_6 + {}^6/_4W + 2Na_2Q + {}^6/_4L \quad (3)$$

Therefore, two out of the eight moles of Na_2Q are redundant. In order to explore this possibility, reactions with different $Na_2Te:W_6Cl_{12}$ mole ratios ($Na_2Te:W_6Cl_{12}$ = 6, 8, 10, 12) were examined in refluxing pyridine. For the larger mole ratios (Na_2-

Te:W_6Cl_{12} = 8, 10, 12), about 40−50% of the tungsten was converted to the soluble anionic product $W_6Te_8(py)_6^-$. The insoluble product was the neutral complex $W_6Te_8(py)_6$. For the 1:6 (W_6Cl_{12}:Na_2Te) reactions, a relatively small amount of material (only 5−15% of W) was soluble, while the major product was the insoluble $W_6Te_8(py)_6$, and no mixed chloride−telluride cluster complexes were detected. Different reaction times (1 day, 3 days, 6 days) were also tested for this 1:6 reaction system, and it was observed that the longer the reaction time, the less amount of soluble material was recovered from the reaction filtrates.

Although an understanding of the mechanism of this process is not completely clear at this stage, we think that the following steps (illustrated in eqs 4−8) are probably involved on the basis

$$W_6Cl_{12} + 8Na_2Te \xrightarrow{L} Na_4W_6Te_8L_x + 12NaCl \quad (4)$$

$$13Na_4W_6Te_8 \xrightarrow{L} 12Na_3W_6Te_8L_x + 6W + 8Na_2Te \quad (5)$$

$$14Na_3W_6Te_8L_x \xrightarrow{L} 13Na_2W_6Te_8L_x + 6W + 8Na_2Te \quad (6)$$

$$15Na_2W_6Te_8L_x \xrightarrow{L} 14NaW_6Te_8L_6 + 6W + 8Na_2Te \quad (7)$$

$$16NaW_6Te_8L_6 \xrightarrow{L} 15W_6Te_8L_6 + 6W + 8Na_2Te \quad (8)$$

of the experimental observations. The overall reaction is illustrated in eq 9. It is conceivable that the $(W_6Te_8L_6)^{4-}$ cluster

$$W_6Cl_{12} + 6Na_2Te \xrightarrow{L} {}^3/_4W_6Te_8L_6 + {}^6/_4W + 12NaCl \quad (9)$$

units were formed as the initial product at an early stage of the substitution reaction. However, in refluxing pyridine, this $(W_6Te_8L_6)^{4-}$ unit may not be thermodynamically or kinetically stable because it undergoes disproportionation to give tungsten metal, Na_2Te, and a trianion salt, eq 5. Further disproportionations can occur consecutively to give the dianion, monoanion, and neutral cluster complexes. The fact that the different oxidized cluster units W_6Te_8 (20e) and $W_6Te_8^-$ (21e) were isolated in these reactions provides the evidence for this mechanism. Unfortunately, tungsten metal was not detected by either XPS or XRD. XP spectroscopy could not differentiate between W metal and W_6Te_8 cluster compounds (see below). The amount of tungsten metal formed is relatively small (~8%) compared with the amounts of other insoluble products, NaCl, Na_2Te, and the neutral cluster $W_6Te_8(py)_6$. Also, the tungsten metal formed by the disproportionation reaction in solution probably has poor crystallinity. Therefore, the results of both XPS and XRD studies on the insoluble products were inconclusive. Only the neutral and the monoanion cluster complexes have been identified. The dianion, trianion, and even the tetraanion cluster complexes may form and remain in the reaction mixture, but these have not been identified. More likely, these anions are unstable with respect to the subsequent disproportionation reactions. The last step, as shown in eq 8, probably is kinetically slow; thus, the sodium salt of the monoanion cluster complex, $NaW_6Te_8(py)_6$, was obtained as a kinetically trapped product. The overall reaction (eq 9) suggests that only 6 mol of Na_2Te is sufficient for complete substitution, and the maximum yield is 75% based upon W_6Cl_{12}.

For the selenide reaction systems, the same mechanism may also be applied. However, no evidence was found that cluster units other than neutral complexes, $W_6Se_8L_6$, were formed.[12] Evidently the $W_6Se_8L_6^-$ anion is less stable for either kinetic or thermodynamic reasons and cannot be isolated with the procedure used here.

Ligand-Exchange Reactions. The complex $W_6Te_8(pip)_6$ could be readily dissolved in neat pyridine to initially form a red solution. After sitting at room temperature for 1 day, the solution turned light brown, and a dark brown solid precipitated. Apparently, the substitution of pyridine for piperidine was achieved, as illustrated in eq 10, and the relatively insoluble

$$W_6Te_8(pip)_6 \xrightarrow{\text{pyridine}} W_6Te_8(py)_6 + 6pip \quad (10)$$

complex, $W_6Te_8(py)_6$ was formed. When $W_6Te_8(py)_6$ was refluxed with excess triethylphosphine in toluene, most of the materials dissolved to form a grape-purple solution within several hours. Single crystals of $W_6Te_8(PEt_3)_6$ were obtained from the solution. Thus, complete substitution of triethylphosphine for pyridine was achieved, as illustrated in eq 11.

$$W_6Te_8(py)_6 + 6PEt_3 \xrightarrow{\text{toluene}} W_6Te_8(PEt_3)_6 + 6py \quad (11)$$

These results illustrated that the bonding between the hexatungsten cluster core and the organic donor ligands appears to have the following order: PEt_3 > py > pip. An identical conclusion was reached in the study of the ligand-exchange reactions among pyridine, piperidine, and triethylphosphine in the sulfide and selenide clusters $M_6Q_8L_6$ (M = Mo, W; Q = S, Se).[5,10b,12]

X-ray Photoelectron Spectroscopy. As previous research has shown,[10c,12] W 4f X-ray photoelectron spectra have provided the most useful spectroscopic data for identification of the W_6Y_8 cluster units. Like their sulfide and selenide analogues, the telluride complexes $W_6Te_8(pip)_6$ and $W_6Te_8(py)_6^{n-}$ (n = 0, 1) show the same tungsten-binding energies, 30.8 eV (W $4f_{7/2}$) and 32.9 eV (W $4f_{5/2}$), which are characteristic values for the tungsten chalcogenide cluster units, W_6Q_8. For comparison, the W $4f_{7/2}$ binding energies for WTe_2 and WO_3 are 32.3 and 35.4 eV, respectively. Therefore, if WTe_2 and WO_3 occur as impurities in the products, distinct evidence for these would be found in the resolved W 4f binding energy values. The W 4f XP spectrum of $W_6Te_8(pip)_6$ could be accounted for nicely by only one major type of tungsten, and no WTe_2 was detected. Since the telluride compounds are very air sensitive, in most cases the presence of surface oxide contamination was evident. Thus, XPS is a useful technique to identify the cluster and detect any impurities in the products. However, XPS was not able to clearly distinguish between tungsten metal and the cluster units, since the W $4f_{7/2}$ binding energy for tungsten metal[23] is nearly the same as that for cluster complexes, 31.4 and 30.8 eV, respectively. The XPS binding energies for cluster units W_6Q_8 and related compounds are tabulated in Table 7.

Infrared Spectra. Infrared spectroscopy has proven to be a powerful tool for the characterization of W_6Te_8 cluster complexes. Characteristic bands for the coordinated organic ligands could be identified in the mid-IR region, and a characteristic band for W−Te, could be observed in far-IR region. The mid-IR and far-IR spectra of the $W_6Te_8(pip)_6$ complex are shown in Figure 1.

Previous studies have resulted in the identification and assignment of these IR bands in the mid-IR region (600−3500 cm^{-1}).[10,12] In the far-IR region, one strong band at about 180

(23) A sample of tungsten metal prepared in this laboratory gave a W $4f_{7/2}$ binding energy of 31.5 eV on the spectrometer described in the Experimental Section. This compares with a reported value of 31.4 eV: *Handbook of X-Ray Photoelectron Spectroscopy*; Perkin-Elmer Corp.: Eden Prairie, MN, 1992; p 173.

Table 7. XPS Binding Energies (eV) for the W_6Q_8 Cluster Complexes and Related Compounds[a]

compd	W $4f_{7/2}$	W $4f_{5/2}$	S $2p_{3/2}$	Se $3d_{5/2}$	Te $3d_{5/2}$
$W_6S_8(py)_6$	30.5	32.6	160.6		
$W_6Se_8(py)_6$	30.8	32.9		53.6	
$W_6Te_8(py)_6$	30.8	32.9			571.9
$W_6S_8(pip)_6$	30.5	32.6	160.6		
$W_6Se_8(pip)_6$	30.8	32.9		53.7	
$W_6Te_8(pip)_6$	30.8	32.9			571.9
WS_2	32.7	34.8	162.4		
WSe_2	32.3	34.4		54.6	
W_6Cl_{12}	32.4	34.5			
W metal	31.4	33.5			

[a] Data have been corrected to the C 1s binding energy of 284.6 eV.

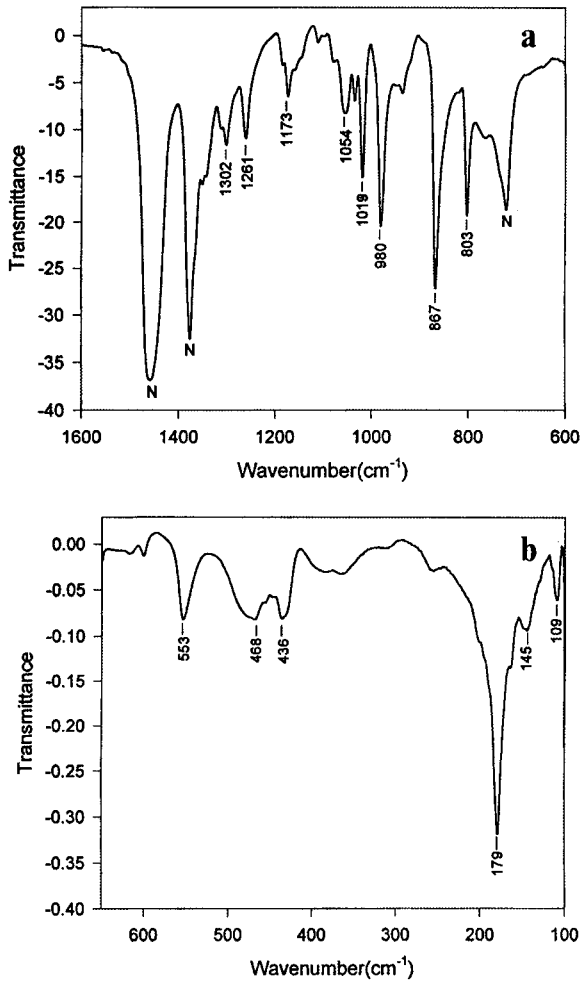

Figure 1. (a) Mid-infrared spectrum of $W_6Te_8(pip)_6$. The bands labeled as "N" are due to Nujol. (b) Far-infrared spectrum of $W_6Te_8(pip)_6$.

cm^{-1} can be assigned as arising from the IR-allowed T_{1u} W−Te stretching modes. The tungsten sulfide and selenide analogues, $W_6S_8(pip)_6$ and $W_6Se_8(pip)_6$, exhibit similar W−S, and W−Se T_{1u} stretching bands at 376 and 243 cm^{-1}, respectively. The reduction from 376 to 240 to 180 cm^{-1} is about the change expected on the basis of reduced masses of the W−Q pairs.

Electronic Spectra. The piperidine cluster complexes $W_6Q_8(pip)_6$ (Q = S, Se, Te) were dissolved in neat piperidine. The sulfide cluster, $W_6S_8(pip)_6$, gave a brown-yellow solution, while the selenide and telluride complexes gave purple and dark blue solutions, respectively. The UV−vis absorption maxima occur at 390, 489, and 566 nm, respectively, for the sulfide, selenide, and telluride complexes. Thus, the absorption peak shifts markedly to higher wavelengths from sulfide to selenide to telluride. The assignment of these absorption bands is not completely clear. However, Saito's DV−Xα MO calculations on $Mo_6Q_8(PH_3)_6$ (Q = S, Se)[24] indicated that those absorptions around 400−500 nm might arise from ligand to metal charge transfer. According to their calculations, the absorption observed around 490 nm for the $Mo_6S_8(PEt_3)_6$ complex was assigned to a ligand-based, low-energy t_{1u} to metal-based e_g (LUMO) transition. Therefore, these absorptions of tungsten chalcogenide cluster complexes can also be attributed to a similar ligand to metal charge transfer. Further EHMO calculations on $W_6Q_8(NH_3)_6$ (Q = S, Se, Te) complexes also indicated that these absorptions arose from ligand to metal charge transfer (see below).

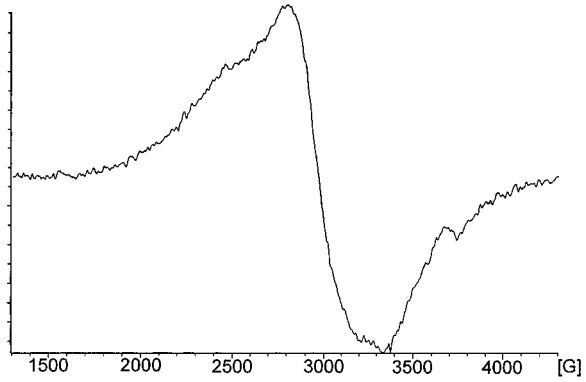

Figure 2. ESR spectrum of $NaW_6Te_8(py)_x$ at 110 K.

ESR Study. After the solid was dried overnight *in vacuo* at room temperature, pyridine associated with the sodium ion in the complex $[Na(py)_6][W_6Te_8(py)_6]\cdot py$ was lost. The recovered black powder was assumed to have a formula close to $NaW_6Te_8(py)_6$. The ESR spectrum of this powdered sample at 110 K is shown in Figure 2. The very broad ESR signal with $g = 2.26$ indicated that the sample contained units with an unpaired electron. Because of the low solubility of this material in organic solvents, a frozen-glass spectrum was not obtained.

Magnetic Measurements. Single crystals of $[Na(py)_6]^+[W_6Te_8(py)_6]^-\cdot py$ were obtained from the filtrate of the 1:8 (W_6Cl_{12}:Na_2Te) reaction in pyridine. Magnetic susceptibility data for material dried under vacuum and assumed to be $NaW_6Te_8(py)_6$ were collected over the range 6−297 K at 5 K intervals in a field of 3 T. The data were corrected for diamagnetic core contributions (-1.08×10^{-3} emu/mol), on the basis of the formula of $NaW_6Te_8(py)_6$, using values for the individual ions reported by Selwood.[25] The molar susceptibility and reciprocal molar susceptibility for this material are shown in Figure 3. The data can be fit by the Curie−Weiss relationship $\chi = C/(T + \Theta) + \chi_{TIP}$ from 6 to 297 K. A linear regression fitting of the observed data yielded $\chi_{TIP} = 5.70 \times 10^{-4}$ emu/mol, $C = 0.028$ emu·K/mol, and $\Theta = -4.33$ K. The magnetic moment calculated from the Weiss constant C is 0.48 μ_B, which is too low for the possibility of one unpaired electron per cluster unit (1.73 μ_B) expected from the formal metal-centered electron count of 21 for the anion $[W_6Te_8(py)_6]^-$. The cause of the very low magnetic moment is not known. It is possible that removal of weakly bound pyridine in crystalline $[Na(py)_6][W_6Te_8(py)_6]\cdot py$ results in extensive loss of the $[W_6Te_8(py)_6]^-$ anion by disproportionation and formation of the more stable 20-electron, neutral complex $W_6Te_8(py)_6$, as indicated in eq 8. Apparently the unique cluster anion in the solvated sodium salt is effectively stabilized by crystallization with the unusual $Na(py)_6^+$ cation. Thus removal of the coordinated pyridine from the latter should destabilize the anion and promote reaction as shown in eq 8.

(24) Imoto, H.; Saito, T.; Adachi, H. *Inorg. Chem.* **1995**, *34*, 2415.
(25) Selwood, P. W. *Magnetochemistry*, 2nd ed.; Interscience Publishers: New York, 1988; p 78.

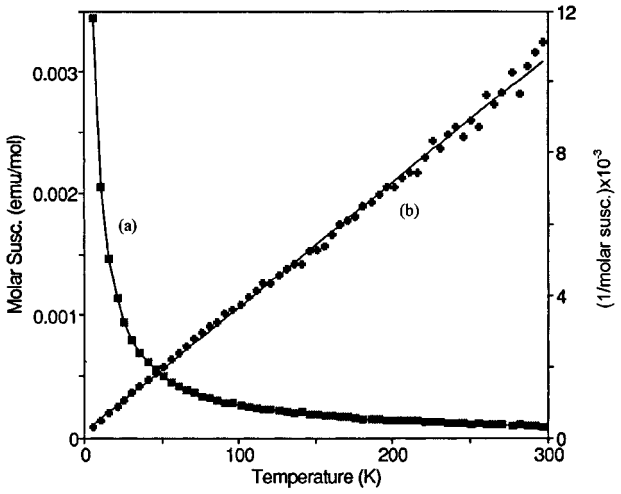

Figure 3. (a) Molar susceptibility versus temperature for $Na[W_6Te_8(py)_6]$. (b) Reciprocal molar susceptibility versus temperature for $Na[W_6Te_8(py)_6]$. The points are experimental data points, and the straight lines are the linear regression fittings.

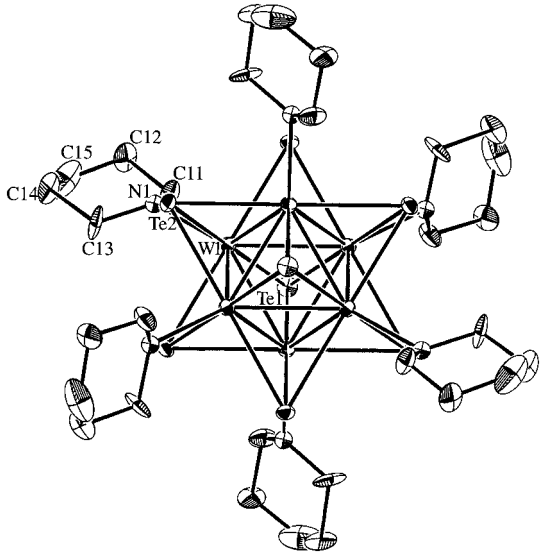

Figure 4. Molecular structure of $W_6Te_8(pip)_6$. Thermal ellipsoids are shown at the 35% probability level. Hydrogen atoms have been omitted for clarity.

Crystal Structures. Both of the neutral molecular complexes reported here contain the hexatungsten cluster unit $W_6Te_8L_6$. This cluster unit can be viewed as an octahedron of tungsten atoms with eight triply-bridging tellurium atoms capping the octahedral faces. Each tungsten also possesses an additional terminal coordination site located at the vertex positions of the octahedron, which are occupied by the organic donor ligands.

$W_6Te_8(pip)_6 \cdot 6pip$ crystallizes in the trigonal space group $R\bar{3}$ with 3 molecules per unit cell. The W_6Te_8 cluster unit is centered on a $\bar{3}$ position (3a site symmetry). It is isomorphous with the $W_6Se_8(py)_6 \cdot 6py$ complex.[12] An ORTEP drawing of the cluster is shown in Figure 4. The piperidine ligand in the chair conformation coordinates to the tungsten atom such that the W−N bond occupies the equatorial position on the N atom. Selected bond distances and bond angles are listed in Table 8.

In comparison with those of the sulfide and selenide analogues, $W_6S_8(pip)_6$[10c] and $W_6Se_8(pip)_6$,[12] the average W−W bond distance of 2.742(2) Å in the telluride cluster is much longer. cf. 2.689(2) Å for $W_6Se_8(pip)_6$ and 2.6588(3) Å for $W_6S_8(pip)_6$. The average W−Te distance of 2.753(2) Å is also much longer than the average W−S distance of 2.461(3) Å in $W_6S_8(pip)_6$ and average W−Se distance of 2.569(3) Å in $W_6Se_8(pip)_6$. The average W−N distance of 2.34(2) Å in these telluride clusters is close to the values found for the sulfide and selenide clusters. A summary of the average bond distances and bond angles in these $W_6Q_8(pip)_6$ (Q = S, Se, Te) complexes is given in Table 9. Besides the changes in W−W and W−Q bond distances, two other notable differences among these chalcogenide cluster units are the average W−Q−W and trans Q−W−Q bond angles. The average trans S−W−S, Se−W−Se, and Te−W−Te bond angles are 173.0(2), 175.9(1), and 180.76(5)°, respectively. Thus, the tungsten atoms reside on the outside of the cube, above the planes formed by the neighboring four chalcogen atoms in both the W_6S_8 and W_6Se_8 units, while in the W_6Te_8 unit, the tungsten atoms reside just slightly below the plane, almost coplanar with the four tellurium atoms. However, for the halide cluster compounds $(M_6X_8)X_4$ (M = Mo, W; X = Cl, Br, I), the metal atom is sitting below the plane which is formed by four halogen atoms. Therefore, the elongation of the metal−metal bond distances in the heavier halide clusters is associated with the larger covalent radius of the heavier halogen atoms. In order to compensate for the larger radius of the heavier halogen atoms, the metal core M_6 has to expand. This effect has been termed as a "matrix effect".[26] In contrast, it is less important for the metal core M_6 to expand for these tungsten chalcogenide clusters. Thus, the elongation of the W−W bond distances in the selenide and telluride clusters can be attributed to both electronic and matrix effects.

$W_6Te_8(PEt_3)_6$ crystallizes in a monoclinic space group, $C2/c$, with 4 molecules per unit cell. The W_6Te_8 cluster unit is

Table 8. Selected Bond Lengths (Å) and Angles (deg) in $W_6Te_8(pip)_6 \cdot 6pip$[a]

W(1)−W(1B)	2.744(2)	W(1)−Te(1)	2.740(2)
W(1)−W(1C)	2.740(2)	W(1)−Te(2)	2.770(2)
av W−W	2.742(3)	W(1)−Te(2C)	2.750(2)
		W(1)−Te(2D)	2.752(2)
W(1)−N(1)	2.34(2)	av W−Te	2.753(2)
C(11)−C(12)	1.52(3)		
C(12)−C(15)	1.47(4)	N(1)−C(11)	1.52(3)
C(13)−C(14)	1.51(3)	N(1)−C(13)	1.40(3)
C(14)−C(15)	1.51(4)		

W(1C)−W(1A)−W(1D)	60.00(3)	W(1)−W(lD)−W(lA)	90.00(4)
W(1)−W(1B)−W(1C)	59.96(4)	W(1B)−W(1)−W(1D)	90.00(4)
W(1C)−W(1)−W(1D)	60.09(4)		
av W−W−W	60.02(5)	Te(1)−W(1)−Te(2C)	89.55(4)
		Te(1)−W(1)−Te(2D)	89.51(3)
W(1)−Te(1)−W(1B)	60.11(5)	Te(2C)−W(1)−Te(2)	90.50(5)
W(1)−Te(2)−W(1C)	59.51(4)	Te(2D)−W(1)−Te(2)	90.45(5)
W(1)−Te(2)−W(1D)	59.54(4)	av Te−W−Te	90.00(5)
W(1)−Te(2C)−W(1B)	59.84(4)		
av W−Te−W	59.75(5)	Te(2)−W(1)−N(1)	86.9(4)
		Te(2C)−W(1)−N(1)	90.5(4)
Te(1)−W(1)−Te(2)	180.25(5)	Te(2D)−W(1)−N(1)	88.7(4)
Te(2D)−W(1)−Te(2C)	181.28(5)	Te(1)−W(1)−N(1)	93.3(4)
av Te−W−Te	180.76(7)	av Te−W−N	89.9(5)

[a] Equivalent atoms generated by symmetry transformation: (A) $-x$, $-y$, $-z$; (B) $-x+y$, $-x$, z; (C) y, $-x+y$, $-z$; (D) $x-y$, x, $-z$.

Table 9. Summary of Selected Average Bond Distances (Å) and Bond Angles (deg) for the $W_6Q_8L_6$ (Q = S, Se, Te) Cluster Complexes

formula	W−W	W−Q	W−L	Q−W−Q	W−Q-W
$W_6S_8(pip)_6$	2.659(1)	2.461(4)	2.31(5)	173.0(2)	65.56(2)
$W_6Se_8(pip)_6$	2.689(2)	2.569(3)	2.27(3)	175.9(1)	63.13(8)
$W_6Te_8(pip)_6$	2.742(3)	2.753(2)	2.34(2)	180.76(7)	59.75(5)
$W_6Te_8(PEt_3)_6$	2.770(2)	2.744(1)	2.536(4)	179.12(4)	60.62(4)
$W_6S_8(PEt_3)_6$	2.673(1)	2.452(3)	2.513(2)	172.5(3)	66.06(7)
$[Na(py)_6][W_6Te_8(py)_6]$	2.732(1)	2.763(1)	2.30(1)	181.18(4)	59.25(3)

(26) Corbett, J. D. *J. Solid State Chem.* **1981**, *37*, 335.

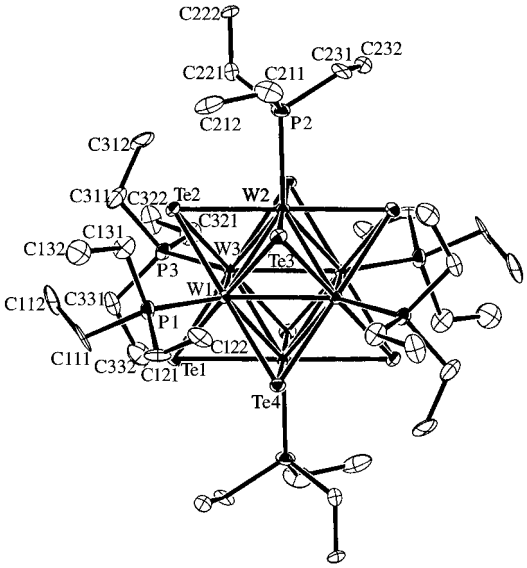

Figure 5. Molecular structure of $W_6Te_8(PEt_3)_6$. Thermal ellipsoids are shown at the 35% probability level. Hydrogen atoms have been omitted for clarity.

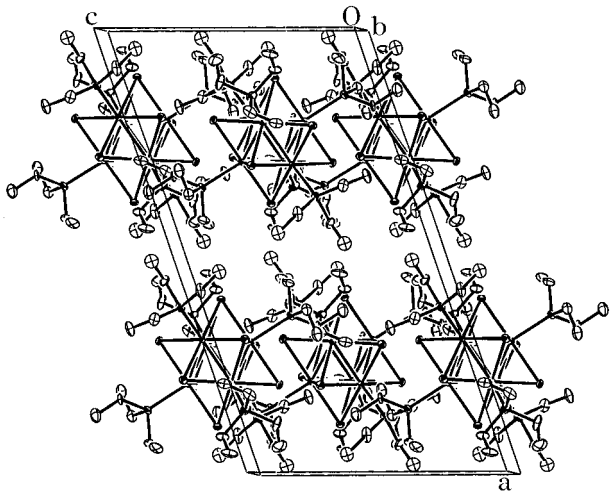

Figure 6. Unit cell packing diagram for $W_6Te_8(PEt_3)_6$ as viewed approximately along the *b* axis. Thermal ellipsoids are shown at the 35% probability level.

Table 10. Selected Bond Distances (Å) in $W_6Te_8(PEt_3)_6$[a]

W(1)−W(2)	2.767(1)	W(1)−Te(1)	2.746(2)
W(1)−W(2A)	2.770(1)	W(1)−Te(2)	2.736(1)
W(1)−W(3)	2.770(2)	W(1)−Te(3)	2.751(2)
W(1)−W(3A)	2.775(1)	W(1)−Te(4)	2.742(1)
W(2)−W(3)	2.765(2)	W(2A)−Te(1)	2.734(1)
W(2)−W(3A)	2.771(1)	W(2)−Te(2)	2.747(1)
av W−W	2.770(2)	W(2)−Te(3)	2.751(2)
		W(2A)−Te(4)	2.750(1)
W(1)−P(1)	2.542(5)	W(3)−Te(1)	2.748(1)
W(2)−P(2)	2.532(5)	W(3)−Te(2)	2.741(1)
W(3)−P(3)	2.535(4)	W(3A)−Te(3)	2.734(2)
av W−P	2.536(6)	W(3A)−Te(4)	2.748(1)
		av W−Te	2.744(1)

[a] Equivalent atoms generated by symmetry transformation: (A) $^1/_2 - x, ^1/_2 - y, -z$.

centered on a $\bar{1}$ position (4c site symmetry). An ORTEP drawing of the cluster and a packing diagram are shown in Figures 5 and 6, respectively, and selected bond distances and bond angles are listed in Tables 10 and 11, respectively. The average W−W, W−Te, and W−P bond distances are 2.770(1), 2.744(2), and 2.536(4) Å, respectively. Because the stronger W−P bonding results in increased electron density in the molecular orbitals which are slightly antibonding with respect to the W−W bonds of the cluster, the W−W distance in this complex, 2.770(1) Å, is longer than that of 2.742(2) Å in $W_6Te_8(pip)_6$. The W−P bond distance of 2.536(4) Å is close to that of 2.513(2) Å in the sulfide analogue, $W_6S_8(PEt_3)_6$.[9,10b]

Table 11. Selected Bond Angles (deg) in $W_6Te_8(PEt_3)_6$[a]

W(2)−W(1)−W(2A)	89.81(3)	W(2)−W(1)−W(3)	59.91(2)
W(3)−W(1)−W(3A)	89.96(4)	W(2)−W(1)−W(3A)	59.99(2)
W(1)−W(2)−W(1A)	90.19(3)	W(2A)−W(1)−W(3)	60.02(3)
W(3)−W(2)−W(3A)	90.16(4)	W(2A)−W(1)−W(3A)	59.81(3)
W(1)−W(3)−W(1A)	90.04(4)	W(1)−W(2)−W(3)	60.09(3)
W(2)−W(3)−W(2A)	89.84(4)	W(1)−W(2)−W(3A)	60.14(2)
av W−W−W	90.00(4)	W(1A)−W(2)−W(3)	60.18(3)
		W(1A)−W(2)−W(3A)	60.14(2)
W(1)−Te(1)−W(2A)	60.71(3)	W(1)−W(3)−W(2)	60.00(4)
W(1)−Te(1)−W(3)	60.54(4)	W(1)−W(3)−W(2A)	59.99(3)
W(2A)−Te(1)−W(3)	60.72(3)	W(1A)−W(3)−W(2)	60.00(3)
W(1)−Te(2)−W(2)	60.63(3)	W(1A)−W(3)−W(2A)	59.86(3)
W(1)−Te(2)−W(3)	60.76(4)	av W−W−W	60.01(3)
W(2)−Te(2)−W(3)	60.50(3)		
W(1)−Te(3)−W(2)	60.39(4)	Te(1)−W(1)−Te(3)	178.54(4)
W(1)−Te(3)−W(3A)	60.79(4)	Te(2)−W((1)−Te(4)	179.53(4)
W(2)−Te(3)−W(3A)	60.68(4)	Te(1A)−W(2)−Te(2)	179.49(4)
W(1)−Te(4)−W(2A)	60.58(4)	Te(3)−W(2)−Te(4A)	178.89(4)
W(1)−Te(4)−W(3A)	60.72(3)	Te(2)−W(3)−Te(3A)	179.49(4)
W(2A)−Te(4)−W(3A)	60.37(3)	Te(1)−W(3)−Te(4A)	178.78(4)
av W−Te−W	60.62(4)	av Te−W−Te	179.12(4)
Te(1)−W(1)−Te(2)	90.26(5)	Te(1)−W(1)−P(1)	91.0(1)
Te(1)−W(1)−Te(4)	89.70(5)	Te(2)−W(1)−P(1)	87.6(1)
Te(3)−W(1)−Te(4)	89.49(5)	Te(3)−W(1)−P(1)	90.3(1)
Te(2)−W(1)−Te(3)	90.54(5)	Te(4)−W(1)−P(1)	92.9(1)
Te(1A)−W(2)−Te(3)	89.55(5)	Te(1A)−W(2)−P(2)	91.3(1)
Te(2)−W(2)−Te(4A)	90.37(5)	Te(2)−W(2)−P(2)	89.2(1)
Te(2)−W(2)−Te(3)	90.30(5)	Te(3)−W(2)−P(2)	92.2(1)
Te(1)−W(2A)−Te(4)	89.78(5)	Te(4A)−W(2)−P(2)	88.7(1)
Te(3)−W(3A)−Te(4)	89.71(4)	Te(1)−W(3)−P(3)	91.5(1)
Te(4A)−W(3)−Te(2)	90.53(4)	Te(2)−W(3)−P(3)	91.0(1)
Te(3A)−W(3)−Te(1)	89.64(4)	Te(3A)−W(3)−P(3)	89.4(1)
Te(1)−W(3)−Te(2)	90.12(4)	Te(4A)−W(3)−P(3)	89.5(1)
av Te−W−Te	90.00(5)	av Te−W−P	90.4(1)

[a] Equivalent atoms generated by symmetry transformation: (A) $^1/_2 - x, ^1/_2 - y, -z$.

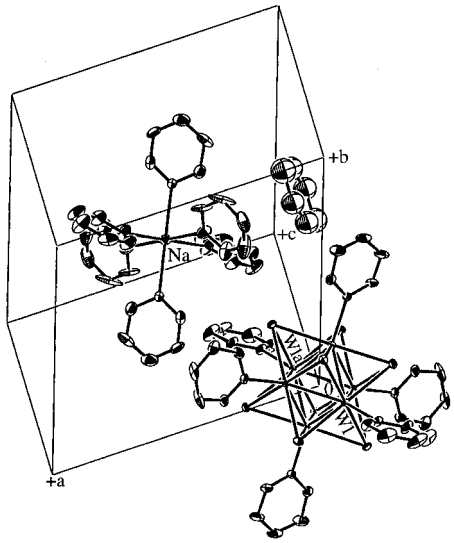

Figure 7. Unit cell of $[Na(py)_6][W_6Te_8(py)_6]\cdot py$ depicted with thermal ellipsoids at the 35% probability level.

$[Na(py)_6][W_6Te_8(py)_6]\cdot py$ crystallizes in the triclinic space group *P*$\bar{1}$ with one molecule per unit cell. A diagram of the unit cell of $[Na(py)_6][W_6Te_8(py)_6]\cdot py$ is shown in Figure 7. As illustrated, the W_6Te_8 cluster anion is centered on the origin of the unit cell (1a site symmetry), the Na^+ cation is located on the center of the unit cell (1h site symmetry) with six pyridine

Table 12. Selected Bond Distances (Å) in $[Na(py)_6][W_6Te_8(py)_6]\cdot py$[a]

W(1)−W(2)	2.742(1)	W(1)−Te(1)	2.748(1)
W(1)−W(2A)	2.729(1)	W(1)−Te(3)	2.764(1)
W(1)−W(3)	2.746(1)	W(1)−Te(2A)	2.767(1)
W(1)−W(3A)	2.733(1)	W(1)−Te(4A)	2.745(3)
W(2)−W(3)	2.723(1)	W(2)−Te(1)	2.757(1)
W(2)−W(3A)	2.718(1)	W(2)−Te(2)	2.763(1)
av W−W	2.732(1)	W(2)−Te(3)	2.777(1)
		W(2)−Te(4)	2.776(1)
W(1)−N(1)	2.31(1)	W(3)−Te(2)	2.762(1)
W(2)−N(2)	2.30(1)	W(3)−Te(3)	2.765(1)
W(3)−N(3)	2.29(1)	W(3)−Te(1A)	2.777(1)
av W−N	2.30(1)	W(3)−Te(4A)	2.756(1)
		av W−Te	2.763(1)
Na(1)−N(10)	2.52(2)		
Na(1)−N(20)	2.63(2)		
Na(1)−N(30)	2.54(2)		
av Na−N	2.56(2)		

[a] Equivalent atoms generated by symmetry transformation: (A) $-x$, $-y$, $-z$.

Table 13. Selected Bond Angles (deg) in $[Na(py)_6][W_6Te_8(py)_6]\cdot py$[a]

W(2)−W(1)−W(2A)	89.19(3)	W(2)−W(1)−W(3)	59.49(3)
W(3)−W(1)−W(3A)	89.38(3)	W(2)−W(1)−W(3A)	59.52(3)
W(1)−W(2)−W(1A)	90.81(3)	W(2A)−W(1)−W(3)	59.52(3)
W(3)−W(2)−W(3A)	90.19(3)	W(2A)−W(1)−W(3A)	59.81(3)
W(1)−W(3)−W(1A)	90.62(3)	W(1)−W(2)−W(3)	60.34(3)
W(2)−W(3)−W(2A)	89.81(3)	W(1)−W(2)−W(3A)	60.08(3)
av W−W−W	90.00(3)	W(1A)−W(2)−W(3)	60.18(3)
		W(1A)−W(2)−W(3A)	60.56(3)
W(1)−Te(1)−W(2)	59.73(3)	W(1)−W(3)−W(2)	60.17(3)
W(1)−Te(1)−W(3A)	59.29(3)	W(1)−W(3)−W(2A)	59.93(3)
W(2)−Te(1)−W(3A)	58.81(3)	W(1A)−W(3)−W(2)	60.02(3)
W(1A)−Te(2)−W(2)	59.13(3)	W(1A)−W(3)−W(2A)	60.40(3)
W(1A)−Te(2)−W(3)	59.26(3)	av W−W−W	60.00(4)
W(2)−Te(2)−W(3)	59.05(3)		
W(1)−Te(3)−W(2)	59.30(3)	Te(1)−W(1)−Te(4A)	181.75(4)
W(1)−Te(3)−W(3)	59.56(3)	Te(3)−W((1)−Te(2A)	180.39(3)
W(2)−Te(3)−W(3)	58.85(3)	Te(1)−W(2)−Te(2)	182.02(4)
W(1A)−Te(4)−W(2)	59.23(3)	Te(3)−W(2)−Te(4)	180.46(4)
W(1)−Te(4A)−W(3)	59.90(3)	Te(2)−W(3)−Te(4A)	181.81(4)
W(2)−Te(4)−W(3A)	58.84(3)	Te(3)−W(3)−Te(1A)	180.65(4)
av W−Te−W	59.25(3)	av Te−W−Te	181.18(4)
Te(2)−W(1A)−Te(4)	90.73(4)	Te(2A)−W(1)−N(1)	88.2(3)
Te(2A)−W(1)−Te(1)	90.67(4)	Te(4A)−W(1)−N(1)	89.6(3)
Te(4A)−W(1)−Te(3)	89.03(4)	Te(1)−W(1)−N(1)	89.5(3)
Te(1)−W(1)−Te(3)	89.55(4)	Te(3)−W(1)−N(1)	91.5(3)
Te(1)−W(2)−Te(3)	89.09(4)	Te(1)−W(2)−N(2)	89.3(3)
Te(1)−W(2)−Te(4)	90.95(4)	Te(2)−W(2)−N(2)	89.0(3)
Te(2)−W(2)−Te(3)	89.79(4)	Te(3)−W(2)−N(2)	91.4(3)
Te(2)−W(2)−Te(4)	90.15(4)	Te(4)−W(2)−N(2)	88.2(3)
Te(1)−W(3A)−Te(4)	90.95(4)	Te(1A)−W(3)−N(3)	89.0(3)
Te(4A)−W(3)−Te(3)	88.79(4)	Te(2)−W(3)−N(3)	89.1(3)
Te(1A)−W(3)−Te(2)	90.16(4)	Te(3)−W(3)−N(3)	90.4(3)
Te(2)−W(3)−Te(3)	90.08(4)	Te(4A)−W(3)−N(3)	89.5(3)
av Te−W−Te	90.00(4)	av Te−W−N	89.6(3)
N(10)−Na−N(20)	94.5(5)	N(10)−Na−N(30)	94.6(5)
N(20)−Na−N(30)	93.8(5)		

[a] Equivalent atoms generated by symmetry transformation: (A) $-x$, $-y$, $-z$.

molecules pseudooctahedrally coordinated to it, and the one free pyridine solvent molecule is centered in the face of the *bc* plane (1g site symmetry). Selected bond distances and bond angles are listed in Tables 12 and 13, respectively.

A distortion of the metal octahedron can be found in the $[W_6Te_8(py)_6]^-$ unit. The main component of this distortion of the metal octahedron is a pseudotetragonal elongation along the W(1)−W(1A) axis: the W(1)−W(1A) distance of 3.895(1) Å is longer than the other two metal−metal distances across the center of the cluster by 0.054(1) and 0.041(1) Å, respectively.

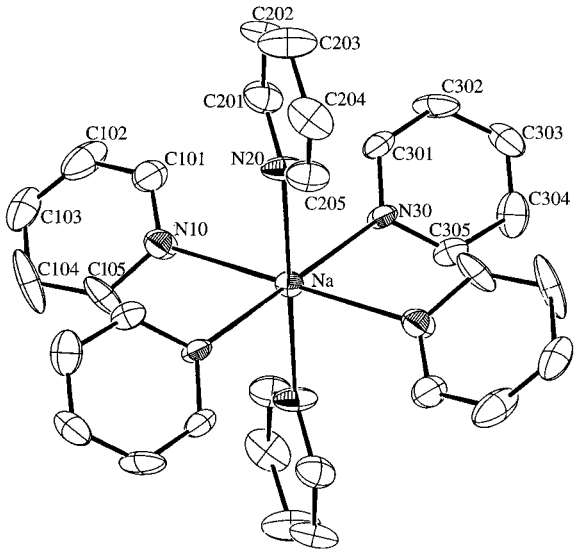

Figure 8. ORTEP drawing of the cation unit $[Na(py)_6]^+$ with thermal ellipsoids at the 35% probability level.

Also, the average W(2)−W(3) bond distance of 2.720(1) Å is noticeably shorter than the average of the W(1)−W(2) and W(1)−W(3) bond distances, 2.737(1) Å. This reduced complex formally has 21 electrons involved in the metal−metal bonding. The distortion may be driven by the Jahn−Teller effect resulting from the HOMO e_g^1 electron configuration and ^2E_g ground state in O_h symmetry. The average W−W and W−Te distances are 2.732(1) and 2.763(1) Å, respectively. In comparison, the neutral complex $W_6Te_8(pip)_6$ has a slightly longer average W−W bond distance, 2.742(2) Å, and a slightly shorter average W−Te bond distance, 2.753(2) Å. The shortening of the W−W bond distances and the elongation of the W−Te bond distances in the reduced anionic complex suggest that the HOMO e_g orbital is metal−metal bonding and metal−tellurium antibonding in nature. EHMO calculations on this tungsten telluride compound lead to a similar conclusion. In contrast, for the molybdenum clusters $[Mo_6Q_8(PEt_3)_6]^{n-}$ (Q = S, Se; $n = 0, 1$),[9] the reduced anionic complexes had slightly longer metal−metal bond distances than those of the neutral complexes, which indicated that the e_g MO's in these systems were slightly antibonding with respect to the metal−metal bonding. This contrasting result for the Mo_6Q_8 clusters is not accounted for in the more sophisticated calculations by the DV−Xα method.[24]

In the interesting and novel $[Na(py)_6]^+$ cation unit, the six pyridine molecules are pseudooctahedrally coordinated to the Na^+ ion as shown in Figure 8. Doedens and Dahl concluded that, in the absence of distortional forces (such as hydrogen bonding or Jahn−Teller degeneracies), a transition metal bound to six identical C_{2v} ligands would presumably exist in the T_h molecular symmetry.[27] However, the overall configuration of the $Na(py)_6^+$ cation is quite different from that of $Fe(py)_6^{2+}$, which has the T_h symmetry, and only resulted in a C_i symmetry. Packing forces may be important in this reduction in symmetry.

After consideration of the statistical errors, the Na−N bond distances are essentially identical, varying from 2.52(2) to 2.63(2) Å, and the average Na−N bond distance is 2.56(2) Å. The summation of the ionic radius for Na^+ and the van der Waals radius for N [$r(Na)_{ion} + r(N)_{vdW} = 0.95 + 1.55 = 2.50$ Å] produces a value that is very close to the experimental value, 2.56 Å. This suggests that the pyridine molecules are very loosely bonded to the sodium cation. The $[Na(NC_5H_5)_6]^+$ cation is to our knowledge the first documented example of a sodium

(27) Doedens, R. J.; Dahl, L. F. *J. Am. Chem. Soc.* **1966**, *88*, 4847.

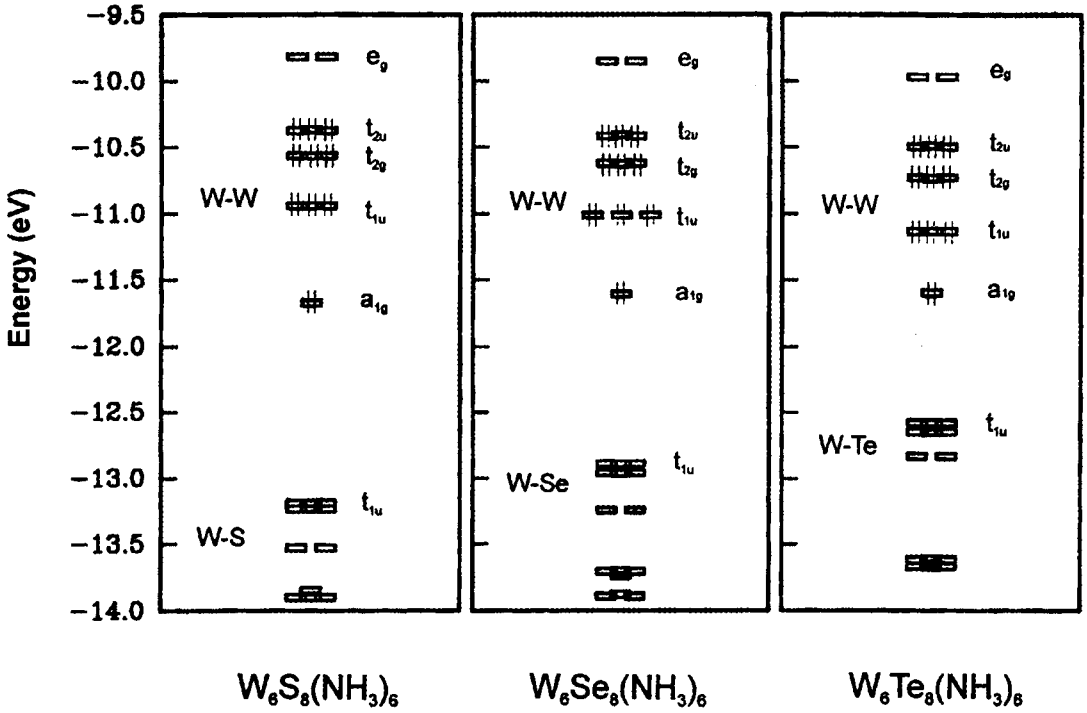

Figure 9. Molecular orbital diagrams for $W_6Q_8(NH_3)_6$ in the HOMO−LUMO region.

ion octahedrally coordinated with six pyridine molecules. The average Na−N distance of 2.56(2) Å in this cation is much longer than the Na−N distances of 2.464(4) and 2.463(5) Å in the compounds $\{[Na(py)_4]_2[Fe_2(CO)_8]\}$[28] and $(C_5Me_5)Na(py)_3$,[29] respectively.

EHMO Calculations. For this series of molecular cluster complexes, $W_6Q_8L_6$ (Q = S, Se, Te), absorption peaks in the electronic spectra shift to higher wavelength from sulfide to selenide to telluride. The crystal structures of $W_6Q_8(pip)_6$ (Q = S, Se, Te) show that the average W−W distances are 2.659(1), 2.689(2), and 2.742(2) Å, respectively. Considering the energy levels of atomic orbitals and electronegativity differences among sulfur, selenium, and tellurium, it was of interest to compare the electronic structures of these complexes as derived from extended Hückel molecular orbital calculations.

The calculated molecular orbital energy diagrams for the metal complexes $W_6Q_8(NH_3)_6$ (Q = S, Se, Te) are shown in Figure 9 for the region just below the LUMO. All three molecular complexes exhibit overall very similar patterns of MO energy levels. The 10 uppermost occupied orbitals are predominantly metal−metal bonding in character, and the reference to these complexes as 20-electron clusters derives from the configuration $a_{1g}^2t_{1u}^6t_{2g}^6t_{2u}^6$ on occupation of these levels. In all cases, the HOMO and LUMO have t_{2u} and e_g symmetries, respectively. The HOMO−LUMO energy gap is nearly constant, *ca.* 0.5 eV, among the three clusters. However, the gap between the lower M−Q bonding t_{1u} MO's (region of −13 eV) and the e_g LUMO's decreases dramatically from 3.37 eV (368 nm) in the sulfide cluster to 3.04 eV (408 nm) and 2.61 eV (475 nm) in the selenide and telluride clusters, respectively. Electronic transitions between these levels are thus ligand to metal (charge transfer) in character and probably correspond to the intense absorptions observed in the UV−vis spectrum of the complexes. The good agreement between these calculated gap energies and the observed transition energies, however, is fortuitous. Finally, we note that the e_g LUMO's also are metal−metal bonding, with some M−Q antibonding character. Thus, occupation of the LUMO with one electron, as in the 21-electron anion $[W_6Te_8(py)_6]^-$, should give the e_g^1 configuration and a ^2E_g ground state subject to a first-order Jahn−Teller distortion. The observed structural distortion and net decrease of the average W−W bond distance in the anion are therefore in agreement with these results of the EHMO calculations.

Acknowledgment. We wish to thank James Anderegg for aid with the XP spectra. This work was supported by The U.S. Department of Energy, Office of Basic Energy Sciences, through Ames Laboratory operated by Iowa State University under Contract No. W-7405-Eng-82.

Supporting Information Available: A complete table of crystallographic data and listings of hydrogen atom coordinates and isotropic thermal parameters and anisotropic thermal parameters for non-hydrogen atoms (10 pages). Ordering information is given on any current masthead page.

IC970037T

(28) Shore, S. G.; Deng, H. *Inorg. Chem.* **1992**, *31*, 2289.
(29) Rabe, G.; Roesky, H. W.; Stalke, D.; Pauer, F.; Sheldrick, G. M. *J. Organomet. Chem.* **1991**, *403*, 11.